nature materials

SUPPLEMENTARY INFORMATION

DOI: 10.1038/NMAT3697

Band alignment of rutile and anatase TiO_2

David O. Scanlon[1],* Charles W. Dunnill[2], John Buckeridge[1],* Stephen A. Shevlin[1], Andrew J. Logsdail[1], Scott M. Woodley[1], C. Richard A. Catlow[1], Michael. J. Powell[2], Robert G. Palgrave[2], Ivan P. Parkin[2], Graeme W. Watson[3], Thomas W. Keal[4], Paul Sherwood[4], Aron Walsh[5], and Alexey A. Sokol[1]*

[1]*University College London, Kathleen Lonsdale Materials Chemistry, 20 Gordon Street, London, WC1H OAJ, UK.*

[2]*Centre for Materials Research, Department of Chemistry, University College London, 20 Gordon Street, London, WC1H 0AJ, UK.*

[3]*School of Chemistry and CRANN, Trinity College Dublin, Dublin 2, Ireland.*

[4]*Scientific Computing Department, STFC, Daresbury Laboratory, Daresbury, Warrington, WA4 4AD, UK.*

[5]*Centre for Sustainable Chemical Technologies and Department of Chemistry, University of Bath, Claverton Down, Bath BA2 7AY, UK.*

Mail to: d.scanlon@ucl.ac.uk, j.buckeridge@ucl.ac.uk, a.sokol@ucl.ac.uk

Electronic structure analysis of the periodic solid:

Calculations were performed using the VASP[1] code, with the projector augmented wave approach[2] used to describe the interaction between the core (Ti:[Ar], O:[He]) and the valence electrons. The calculations were performed using the screened hybrid functional as proposed by Heyd, Scuseria and Ernzerhof (HSE06)[3] in which a percentage (25%) of exact nonlocal Fock exchange is added to the Perdew, Purke and Ernzerhof[4] functional with a screening of $\omega = 0.11$ Bohr^{-1} applied to partition the Coulomb potential into long range and short range terms. The HSE approach consistently produces structural and band gap data that are more accurate than standard density functional approaches, such as the local density approximation (LDA) or the generalized gradient approximation (GGA). Structural optimizations of bulk rutile and anatase TiO_2 were performed using HSE06 at a series of volumes in order to calculate the equilibrium lattice parameters. In each case the atomic positions, lattice vector and cell angle were allowed to relax (within the space group symmetry), while the total volume was held constant. The resulting energy volume curves were fitted to the Murnaghan equation of state to obtain the equilibrium bulk cell volume.[5] This approach minimizes the problems of Pulay stress and changes in basis set which can accompany volume changes in plane wave calculations. The Pulay stress affects the stress tensor which is not used in obtaining the optimized lattice vectors and hence this approach is significantly more accurate than using the stress tensor to perform constant pressure optimization. A cutoff of 500 eV, and k-point meshes of 4×4×6 and 6×6×2, both centered on the Γ point, were found to be sufficient for rutile and anatase, respectively, and all calculations were deemed to be converged when the forces on all atoms were less than 0.01 eV Å^{-1}.

Calculation of band offsets using the method of interatomic potentials:

Band offsets from onsite electrostatic potentials.

In our calculation of onsite electrostatic potentials – Madelung potentials – we have used the accurate room temperature crystallographic data available for both anatase and rutile.[6] Traditionally, in the first instance, a simple rigid ion model is used, in which a formal point charge represents each ion in the system. For a molecule, the electrostatic potential on each ion can be readily evaluated, and typically a reference energy (or level) is *chosen* to be zero when all interatomic distances are infinite. Moreover, this is a *common* reference energy for different molecules thus enabling energetic comparisons. For ions in a unit cell – simulation box

DOI: 10.1038/NMAT3697

with periodic boundary conditions applied in all three directions – there are ions at infinity so care must be taken in evaluating the Madelung potential and in defining a common reference energy. Both problems can be solved, for real life charge-neutral systems, using an Ewald technique.[7] The reference energy for the on-site Madelung potential is when the ion from this site is isolated from the rest of the system; this can be visualised as the ion being displaced to outside of a macroscopic crystal sample, with zero values of total charge and lower multipoles – a model sometimes referred to as a crystal wrapped in metal foil.

As oxide ions are strongly polarisable, the rigid ion model is unable to model qualitatively O ions that are not located at centres of inversion, which is the case for both rutile and anatase phases of titania. The onsite electrostatic field calculated on O ion sites is essentially nonzero. In this field oxygen ions are polarised forming local dipoles, which we need to include in our simulations as this in turn changes the Madelung potential and field on each ion in the system. A model that can account for polarisability of ions, and is employed by us, is the semi-classical polarizable shell model of Dick and Overhouser;[8,9] two point charges (referred to as a core and shell) connected by a harmonic spring represent each ion. The value of the spring constant and how the charge is distributed between the core and shell control the ion polarisability and are fitted to reproduce the high frequency dielectric response of TiO_2.[10] After fitting, only the positions of shells, which represent valence electrons, are relaxed, ensuring the consistency of the induced dipoles and Madelung fields.

For the bulk unit cells, we calculate the Madelung potential centred on the core of an O ion, after relaxation of the shells, multiply this by -1 (charge of an electron), and this product influences the position of the valence band edge. The comparison of the computed values for the two phases results in the valence band offset to the first approximation. A similar procedure is done for the core of the Ti ion yielding the offset for the edge of the conduction band.

Band offsets from defect Mott-Littleton calculations.

In this work, to compare the charge carrier energies propagating at the edges of the valence and conduction bands in rutile and anatase, we calculated electronic relaxation in response to placing an electron on a Ti ion and a hole on an O ion (cf. an early study of alkali halides by Mahan[11,12]). To simulate both carriers we modified the shell charges of respective ions by a unit and then relaxed the position of the shells around the resultant electronic defects. In the Mott-Littleton approach,[13] implemented in the GULP software, by Gale,[14] we input two radial cut-offs that define the boundaries between three spherically concentric regions centred on the defect. In each region a different level of description is employed: shell relaxation is conducted explicitly within the inner sphere; implicitly using harmonic (or linear response) approximation within the middle layer, and only lattice summations of the electrostatic terms (no short range interactions) to infinity in the outer region. The defect energies were converged to 0.01 eV with cut-off radii of 20 Å and 35 Å, respectively – the short range cut-off was set to 15 Å, *i.e.* not greater than the thickness of the middle layer.

QM/MM calculation of rutile and anatase ionisation potentials

A hybrid quantum mechanical / molecular mechanical (QM/MM) embedded cluster approach has been used to determine the ionisation potentials of both rutile and anatase, relative to the vacuum level. The details of this approach have been discussed extensively elsewhere[15-17]; here we give a brief overview.

We represent a part of a crystal by a molecular cluster, treated at a QM level of theory (QM region in Fig. 3(a) of the main text). This cluster is embedded in an external potential, which represents the system remainder (treated at a MM level of theory), thus allowing us to model an infinite system. Screening of charge in the QM cluster is treated explicitly in a surrounding region of radius R (MM active in Fig. 3(a)), exploiting the accurate representation of electronic polarisation in our MM model. A further surrounding region (MM frozen in Fig. 3(a)) is polarised through long-range electrostatic forces determined using Jost's formula[18]:

$$E_{pol} = -\frac{Q^2}{2R}\left(1-\frac{1}{\varepsilon}\right)$$

Here E_{pol} is the polarisation energy, Q is the net charge in the QM region and ε is the trace of the dielectric tensor divided by three. The extent of this frozen MM region is determined by the interatomic potential cut-off. We surround the entire cluster by point charges, the charges of which are fitted in order to reproduce the Madelung potential of the infinite solid in the active region of the model.

Mutual self-consistency in the electronic polarisation effects between the QM and MM regions is achieved by a series of micro-iterations, implemented in the ChemShell package[15,17]. ChemShell provides an interface between QM and MM drivers. We have used the Gamess-UK code[19] for the QM calculations, and GULP[14] for the MM calculations.

By calculating the difference between the total energy of a bulk system in the neutral and positively charged states, where only electronic degrees of freedom are relaxed, we can determine the energy of vertical ionisation, i.e. the ionisation potential (IP). We have used this approach to calculate the IPs of TiO_2 in the rutile and anatase phases.

The QM cluster was treated using density functional theory (DFT) with a triple-zeta valence plus polarisation Gaussian basis set.[20,21] Electron exchange and correlation were treated at the level of hybrid meta-GGA, as parametrised in the BB1k formalism[22]. Embedding of the electronic density within the surrounding MM region was achieved by placing a semi-local effective core potential (ECP)[23] on cation sites in an interface, of 5 Å thickness, between the QM and MM regions. The parametric form of the ECP used was determined as follows. Using the same level of DFT as used in treating our QM cluster, we determined the charge density ρ and Hartree potential of an isolated Ti^{4+} ion. By subtracting the long-range Coulomb term from the Hartree potential, and using ρ to determine the exchange and correlation potential in the local density approximation,[24] we calculated the short-range potential of the Ti^{4+} ion. We then performed a least-squares fitting of a Gaussian function to this potential, in order to reproduce the tail of the potential in the region surrounding the ion, at a distance between 0.5 and 2.2 Å from the ion. This is the region of interest when considering bonding between oxygen and titatnium in TiO_2. The resulting Gaussian function was of the form $0.935e^{-0.356r^2}$. This function was then used as the local part of our ECP, with all non-local parts set to zero. We found that this form of the embedding potential gave a marked improvement over the standard approach, which is to place a large core ECP (taken from the literature) on cation sites in the interface region,[15] by significantly reducing the scatter in energy of deep core states. More details on this approach to the embedding of QM clusters will be published elsewhere.

To calculate the IP of rutile (anatase), we used two QM cluster sizes consisting of 55 and 71 (47 and 79) ions. The active region radius was R = 15 Å, with the frozen region extending a further 15 Å from the centre of the model. The IP of rutile (anatase) was determined to be 7.83 eV (8.30 eV). The IPs calculated using the two QM cluster sizes differed by less than 1\%, indicating that our results are well converged. We calculate a band offset of 0.47 eV between rutile and anatase, with anatase lying below rutile (this trend is also observed using the standard approach to the embedding of QM clusters, mentioned above). This is in good agreement with our experimental result of 0.39 +/- 0.02 eV. Moreover, using experimental values of the bandgap of rutile and anatase (see main text), we determine the electron affinity of rutile (anatase) to be 4.83 eV (5.10 eV). This is in good agreement with the experimentally determined work function of rutile (anatase), 4.9 eV (5.1 eV).[25]

Rutile/Anatase composite synthesis:

Samples consisting of TiO_2 particles containing anatase and rutile junctions were prepared using sol gel techniques. A TiO_2 sol was prepared as follows: Acetylacetone (0.025 mol: 2.52 g) was added to butan-1-ol (32 cm^3), followed by titanium n-butoxide (0.05 mol: 17.50 g) and left to stir vigorously for 1 hour at room temperature. Isopropranol (0.15 mol: 9.05 g) dissolved in water (3.64 ml) was added to the mix and stirred for another hour. Finally, acetonitrile (0.04 mol: 1.66 g) was added to the solution and stirred for 1 hour to

DOI: 10.1038/NMAT3697

complete the preparation for the sol. A layer of rutile was deposited on to a sodium chloride substrate by dip coating the sol and annealing at 700 ^{o}C for 18 h. A subsequent layer of anatase was then deposited on to the sodium chloride / rutile substrate by dip coating the sol and annealing at 500 ^{o}C for 1 h. The substrate was dissolved away using water and the powdered residue retained for analysis using sequential washes and centrifuging. 10 25 mm disk substrates were combined to provide a few mg of material for analysis. A double layer of rutile single layer of anatase was also prepared to give samples with approximately twice the rutile content than the anatase content.

The results from a fragment that survived the removal from the preparative disk showed a difference between the top and bottom side of the thin film recovered from the substrate, Figure. The top side matches perfectly with the expected peak positions[26] of anatase while the bottom surface showed rutile indicating that the materials are indeed anatase rutile layers connected together.

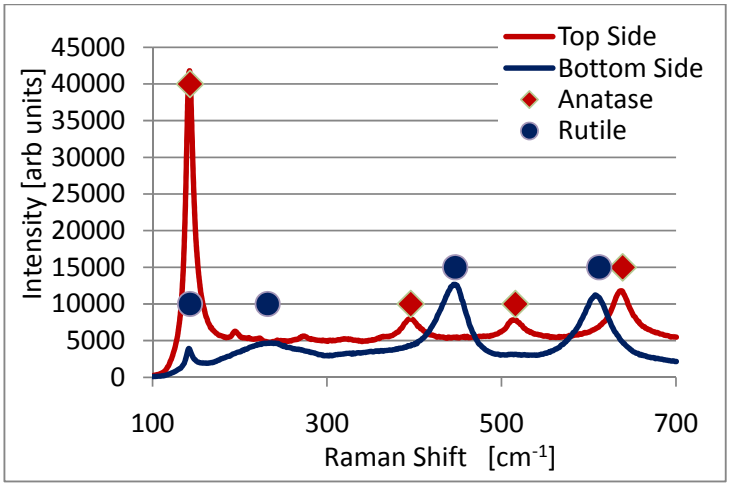

Figure S1: Raman spectra, comparing the materials of the top and bottom of the disk recovered in sample R-A.

SEM micrographs (Figure S2) of the fragile sheeting material analyzed by the Raman shows the layered materials and the tendency of the bulk material to sheer vertically rather than horizontally, i.e to break into composite particles rather than into a mixture of separate anatase and rutile particles. The layered structure is clearly visible with the deep fissures allowing for the easy separation of the disks into particulate materials. Measurements on the micrographs estimate the layer thicknesses to be ~100 nm in agreement with previous research. The area of sheet analysed is made up of a number of pillars that will break up to form particles. The pillar size is approximately ~4 μm in diameter and observed to be flat on top with shelved edges. The deep fissures are known to be typical with sol-gel materials and are due to the thermal shock of the substrate and thin film expanding and contracting at different rates as it heats and cools.

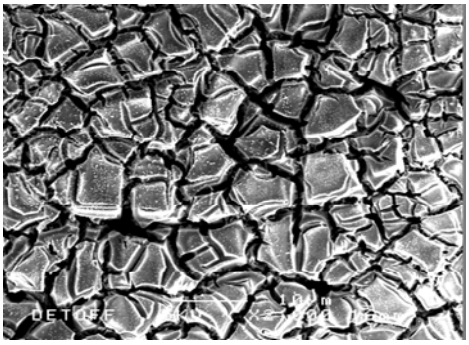

Figure S2: SEM micrograph showing the topology of the A-R sample.

Measurement of band offsets using X-ray Photoelectron Spectroscopy:

X-ray photoelectron spectroscopy (XPS) was used to determine the band offsets in the two phase composite particles using the well-established method of Kraut et al. In this method the energy difference between a core line (CL) and the valence band maximum (VBM) is first measured for the individual components of the composite in isolation. Then by measuring the difference between the CLs in the composite material, the band alignment and energy offset can be determined according to equation 1.

$$\Delta E_{VBM} = \left(E_{CL}^{Rutile} - E_{VBM}^{Rutile}\right) - \left(E_{CL}^{Anatase} - E_{VBM}^{Anatase}\right) - \Delta E_{CL} \quad (1)$$

where E_{CL}^{Rutile} and $E_{CL}^{Anatase}$ are the energy of the Rutile and Anatase core lines respectively, E_{VBM}^{Rutile} and $E_{VBM}^{Anatase}$ are the energies of the Rutile and Anatase VBMs respectively. $\Delta E_{CL} = E_{CL}^{Rutile} - E_{CL}^{Anatase}$ and $\Delta E_{VBM} = E_{VBM}^{Rutile} - E_{VBM}^{Anatase}$. This methodology is commonly applied to determine the band offsets in film-substrate interfaces. For this to be practical, the film thickness must be smaller than the mean free path of photoelectrons in a solid, (which varies with electron energy but is approximately 2.0 nm) since photoelectrons must be recorded from both the film and the underlying substrate. In this work we use the technique to determine the band offsets in particles with a well-defined heterojunction. Here the thickness limitation is lifted, as for a large number of powder particles in random orientation ensures that both rutile and anatase phases will be within the analysis depth of the instrument whilst in electrical contact with each other.

XPS was carried out using a Thermo Kalpha spectrometer using monochromated Al K alpha radiation, a dual beam charge compensation system and a constant pass energy of 50 eV. Phase pure samples of anatase and rutile powder supplied by Sigma Aldrich were measured to obtain the energy difference between the $Ti2p_{3/2}$ CL and the VBM, and also the peak shape of the $Ti2p_{3/2}$ CL for each polymorph. The energy of the VBM was determined by extrapolating the linear portion of the low energy edge of the valence band to the spectral baseline, the latter determined by taking an average of the intensity at binding energies more negative than -3 eV, representing the level of instrument noise at an energy where there is no photoemission intensity. Linear extrapolation of the VB edge allows facile empirical determination of the VBM energy. However, spectral broadening from intrinsic and experimental factors may cause the VBM values obtained to be slightly smaller than those obtained from other techniques, such as electrochemical measurements. However, since the method used here to determine band offsets relies only on energy differences, not absolute energies, a small systematic error in the VBM energies does not affect the calculated offsets.

Using this technique it was determined that $E_{VBM}^{Anatase}$ = 2.77 eV and E_{VBM}^{Rutile} = 2.61 eV, when using the adventitious C 1*s* peak set to 285.00 eV for charge correction. Since the zero point of the binding energy scale corresponds to the Fermi Level (E_F), the position of the VBMs relative to E_F show that as expected both anatase and rutile samples are n-type semiconductors.

Using this method the energy difference between the $Ti2p_{3/2}$ CL and the VBM for anatase was 456.19 eV and for rutile was 456.14 eV. The anatase $Ti2p_{3/2}$ CL was fitted with a single curve formed from a 30.6 : 69.4 Gaussian-Lorentzian product with FWHM of 0.99 eV on a Shirley background. The rutile $Ti2p_{3/2}$ CL was fitted with a single curve formed from a 28.4:71.6 Gaussian-Lorentzian product with FWHM of 1.09 eV on a Shirley background.

The Ti $2p_{3/2}$ spectra from the composite materials were used to ascertain the CL separation and, using equation 1, calculate the valence band offsets. The Ti 2*p* spectrum of TiO_2 can be broadened by the presence of a hydroxylated surface, which creates Ti environments with distinct binding energies. Such broadening would interfere with the attempted analysis, so to rule this possibility out, the O 1*s* spectrum was recorded for each sample. In each case the area of the OH component was less than 6% of the O 1*s* peak. Thus the Ti 2*p* peak is expected to contain only a very small contribution from hydroxylated Ti environments. Based on the structure of the two phase composite particles, the $Ti2p_{3/2}$ spectrum will consist of two components,

DOI: 10.1038/NMAT3697

originating from Ti ions in the rutile and anatase phases. The Ti $2p_{3/2}$ spectra from composite materials of three compositions (Rutile:Anatase 2:1, 1:1, 1:2) were fitted with the anatase and rutile components of peak shape and FWHM constrained to those of the pure phases (Figure S3, and details given above). The peak area ratio was constrained to the expected rutile:anatase composition for each sample. Thus with the component peak shape, area and FWHM constrained, the only parameter varied was the component separation, which was unconstrained. The goodness of fit was determined by the normalised residual standard deviation (RSD). When plotted against component separation, the RSD showed two minima, corresponding to either the Rutile or Anatase component at higher binding energy. In all cases the model gave a better fit to the data (lower RSD) when the anatase component was at higher binding energy. The energy difference between these components (ΔE_{CL}) was used to determine the valence band offset between rutile and anatase according to equation 1, and these results are shown in Table S1

Sample Rutile:Anatase ratio	RSD (anatase high BE)	RSD (rutile high BE)	ΔE_{CL} / eV	ΔE_{VBM} / eV
2:1	0.0088	0.0120	-0.48	-0.43
1:1	0.0168	0.0238	-0.43	-0.38
1:2	0.0241	0.0278	-0.42	-0.37

Table S1. Residual standard deviations (RSD) for Ti $2p_{3/2}$ models with the anatase component at higher binding energy (BE) compared with the alternative model with the rutile component at higher BE. The ΔE_{CL} and ΔE_{VBM} values for the better fitting model are also shown.

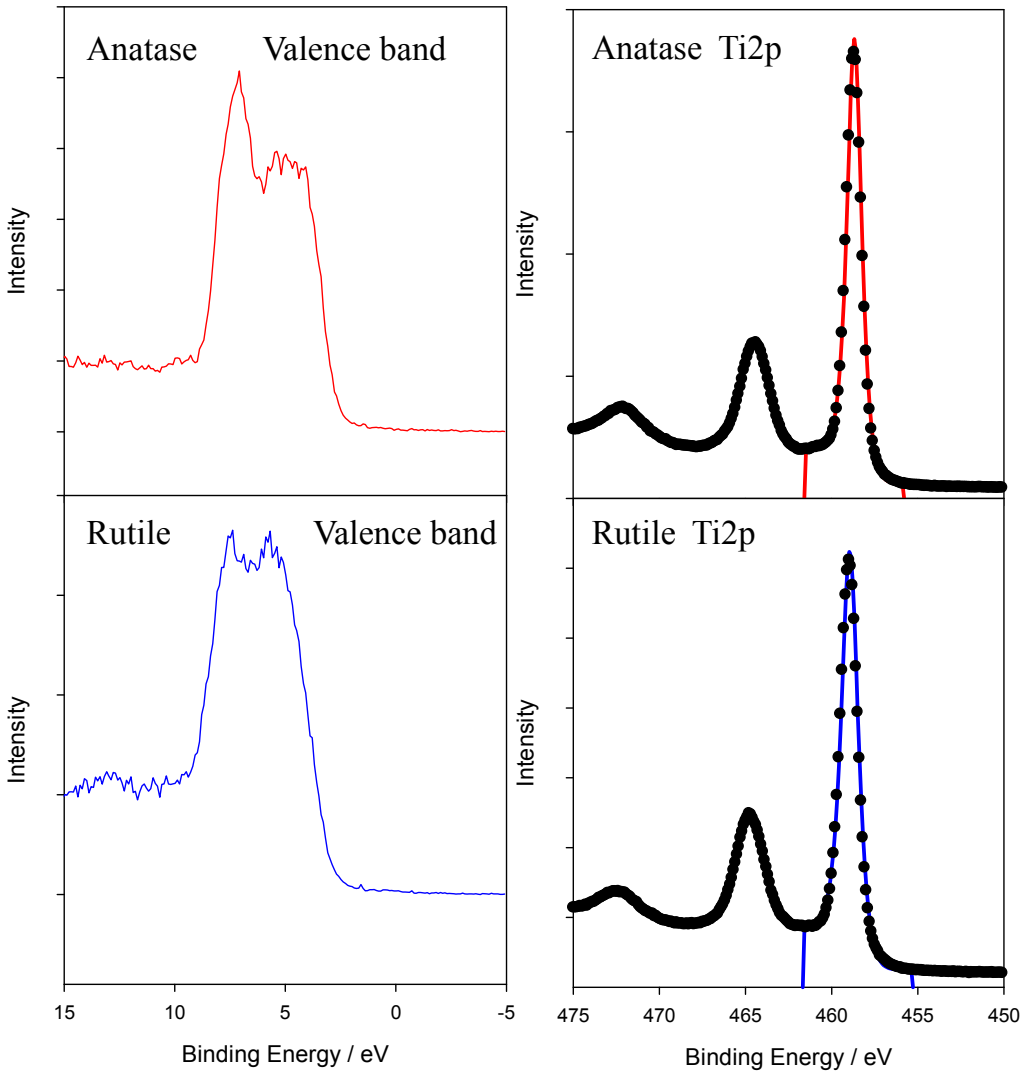

Figure S3. Valence band and Ti2p X-ray photoelectron spectra taken from phase pure anatase and rutile samples. In each case the $Ti2p_{3/2}$ component of the core line is fitted with a single Gaussian-Lorentzian function – for details see text.

1 Kresse, G. & Hafner, J. Ab-Initio Molecular-Dynamics Simulation of the Liquid-Metal Amorphous-Semiconductor Transition in Germanium. *Phys Rev B* **49**, 14251-14269 (1994).

2 Blöchl, P. E. Projector Augmented-Wave Method. *Phys. Rev. B* **50**, 17953 (1994).

3 Krukau, A. V., Vydrov, O. A., Izmaylov, A. F. & Scuseria, G. E. Influence of the exchange screening parameter on the performance of screened hybrid functionals. *J Chem Phys* **125** (2006).

4 Perdew, J. P., Burke, K. & Ernzerhof, M. Generalized gradient approximation made simple. *Phys. Rev. Lett.* **77**, 3865 (1996).

5 Murnaghan, F. D. The compressibility of media under extreme pressures. *P Natl Acad Sci USA* **30**, 244-247, doi:DOI 10.1073/pnas.30.9.244 (1944).

6 Howard, C. J., Sabine, T. M. & Dickson, F. Structural and Thermal Parameters for Rutile and Anatase. *Acta Crystallogr B* **47**, 462-468, doi:Doi 10.1107/S010876819100335x (1991).

7 Ewald, P. P. The calculation of optical and electrostatic grid potential. *Ann Phys-Berlin* **64**, 253-287 (1921).

8 Dick, B. G. & Overhauser, A. W. Theory of the Dielectric Constants of Alkali Halide Crystals. *Physical Review* **112**, 90 (1958).

9 Catlow, C. R. A. *et al.* Advances in Computational Studies of Energy Materials. *Philos. Trans. R. Soc. A-Math. Phys. Eng. Sci.* (2010).

10 Errera, J. & Ketelaar, H. Relation between the optical and dielectrical properties - Ionic polarisation in solid bodies. *J Phys-Paris* **3**, 239-247, doi:DOI 10.1051/jphysrad:0193200306023900 (1932).

11 Mahan, G. D. Photoemission from Alkali-Halides - Energies and Line-Shapes. *Phys Rev B* **21**, 4791-4803, doi:DOI 10.1103/PhysRevB.21.4791 (1980).

12 Foot, J. D., Colbourn, E. A. & Catlow, C. R. A. Computer-Simulation of Alkali-Metal Trapped Hole Defects in Alkaline-Earth Oxides. *J Phys Chem Solids* **49**, 1225-1232, doi:Doi 10.1016/0022-3697(88)90180-1 (1988).

13 Mott, M. F. & Littleton, M. J. Conduction in polar crystals. I. Electrolytic conduction in solid salts. *T Faraday Soc* **34**, 0485-0499 (1938).

14 Gale, J. D. GULP: A computer program for the symmetry-adapted simulation of solids. *J Chem Soc Faraday T* **93**, 629-637, doi:Doi 10.1039/A606455h (1997).

15 Sokol, A. A., Bromley, S. T., French, S. A., Catlow, C. R. A. & Sherwood, P. Hybrid QM/MM embedding approach for the treatment of localized surface states in ionic materials. *Int J Quantum Chem* **99**, 695-712 (2004).

16 Sokol, A. A. *et al.* Point defects in ZnO. *Faraday Discuss* **134**, 267-282 (2007).

17 Sherwood, P. *et al.* QUASI: A general purpose implementation of the QM/MM approach and its application to problems in catalysis. *J Mol Struc-Theochem* **632**, 1-28 (2003).

18 Jost, W. Diffusion and electrolytic conduction in crystals (ionic semiconductors). *J Chem Phys* **1**, 466-475, doi:Doi 10.1063/1.1749319 (1933).

19 Guest, M. F. *et al.* The GAMESS-UK electronic structure package: algorithms, developments and applications. *Mol Phys* **103**, 719-747, doi:Doi 10.1080/00268970512331340592 (2005).

20 Weigend, F. & Ahlrichs, R. Balanced basis sets of split valence, triple zeta valence and quadruple zeta valence quality for H to Rn: Design and assessment of accuracy. *Phys Chem Chem Phys* **7**, 3297-3305, doi:Doi 10.1039/B508541a (2005).

21 Bergner, A., Dolg, M., Kuchle, W., Stoll, H. & Preuss, H. Ab-Initio Energy-Adjusted Pseudopotentials for Elements of Groups 13-17. *Mol Phys* **80**, 1431-1441, doi:Doi 10.1080/00268979300103121 (1993).

22 Zhao, Y., Lynch, B. J. & Truhlar, D. G. Development and assessment of a new hybrid density functional model for thermochemical kinetics. *J Phys Chem A* **108**, 2715-2719, doi:Doi 10.1021/Jp049908s (2004).

23 Igel-Mann, G. Doktorarbeit thesis, (1987).

24 Kohn, W. & Sham, L. J. Self-Consistent Equations Including Exchange and Correlation Effects. *Phys Rev* **140**, 1133-& (1965).

25 Xiong, G. *et al.* Photoemission electron microscopy of TiO2 anatase films embedded with rutile nanocrystals. *Adv Funct Mater* **17**, 2133-2138 (2007).

26 Burgio, L. & Clark, R. J. H. Library of FT-Raman spectra of pigments, minerals, pigment media and varnishes, and supplement to existing library of Raman spectra of pigments with visible excitation. *Spectrochimica Acta Part A* **57**, 1491-1521 (2001).